Hydrogen embrittlement mechanism in fatigue and fracture

Yukitaka Murakami [1* 2]

[1] International Institute for Carbon-Neutral Energy Research (WPI-I^{2}CNER), Kyushu University, 744 Moto-oka, Nishi-ku, Fukuoka, 819-0395 Japan

[2] Research Center for Hydrogen Industrial Use and Storage (HYDROGENIUS), National Institute of Advanced Industrial Science and Technology (AIST) 744 Moto-oka, Nishi-ku, Fukuoka, 819-0395 Japan

[*] murakami.yukitaka.600@m.kyushu-u.ac.jp

Keywords: Fatigue, Hydrogen embrittlement, Crack growth mechanism, Load frequency, Hydrogen content, Low, Medium and High strength steels, Aaustenitic stainless steels

Abstract. This paper overviews the recent progress of the experimental study on hydrogen embrittlement (HE) carried out at HYDROGENIUS and I^{2}CNER. The effect of hydrogen on fatigue crack growth rate was strongly dependent on load frequency both in BCC and FCC metals.
The well known term 'hydrogen embrittlement (HE)' expresses undesirable effects due to hydrogen such as loss of ductility, decreased fracture toughness, and degradation of fatigue properties of metals. However, the experimental results on austenitic stainless steels with supersaturated hydrogen show, surprisingly, that hydrogen can have an effect against HE. A dramatic phenomenon was found in which charging a supersaturated level of hydrogen into specimens of austenitic stainless steels drastically improved the fatigue crack growth resistance.
A new inclusion rating method based on the positive use of HE phenomenon is proposed. In case of high strength steels, it is possible to find the maximum inclusion contained in a specimen by simple tensile test using hydrogen pre-charged specimen. The fracture occurs from the maximum inclusions due to HE. The statistics of extremes distribution of the maximum inclusions completely coincided with the data obtained by fatigue test.

1. Introduction

In order to enable the ''hydrogen society (or hydrogen economy)" in the near future, a number of pressing technical problems must be solved. One important task for mechanical engineers and material scientists is the development of materials and systems which are capable of withstanding the effects of cyclic loading in hydrogen environments. In the past, most research on HE over the past 40 years has paid insufficient attention to two points that are crucially important in the elucidation of the true mechanism. One is that, in most studies, the hydrogen content of specimens was not directly measured. Second, detailed studies that have quantified the influence of hydrogen on fatigue crack growth behaviour, based on microscopic observations are very rare; most studies have only examined the influence of hydrogen on tensile properties. In order to produce components which must perform satisfactorily in service for up to 15 years in hydrogen economy, there is an urgent need for basic, reliable data on the fatigue behaviour of candidate materials in hydrogen environments.

2. Materials and experimental methods

2.1 Materials and specimens

The materials overviewed in this paper are pipeline steels, a CrMo steel, three austenitic stainless steels and a bearing steel. Fig.1(a) and (b) shows the shape and dimension of fatigue specimens.

2.2 Method of hydrogen charging

Hydrogen was charged into the specimens either by soaking them in a 20% ammonium thiocyanate solution (NH4 SCN) or by cathodic charging or by exposure to high pressure hydrogen gas.

2.3 Method of fatigue testing

Fatigue tests of the H-charged and uncharged specimens were carried out at room temperature in laboratory air or in hydrogen gas. The tension-compression fatigue tests were conducted at a testing frequency *f* between 0.0015 Hz and 20 Hz.

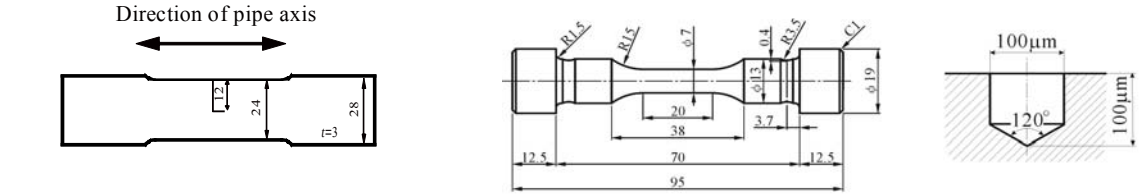

(a) Shape and dimensions of specimens ; dimensions in mm. (Low carbon p ipline steel)

(b) Tension-compression specimen

(c) Small artificial hole

Fig.1. Dimensions, in mm, of the fatigue test specimen and drilled hole introduced to specimen(b). Unit in mm.

3. Results and discussion

3.1 The basic mechanism of void growth in tensile test which is essential also in fatigue

The H-charged specimens show a peculiar void growth inside the specimen in tensile test. Fig. 2 shows an interesting difference of void growth behaviour between the uncharged specimen (Fig.2(a)) and the H-charged specimen (Fig.2(b)) in a pipeline steel[1]. The basic mechanism of the void growth lateral to tensile axis in the H-charged specimen (Fig.2(b) and (c)) can be considered consistent with that of fatigue crack growth(FCG) (Fig.11).

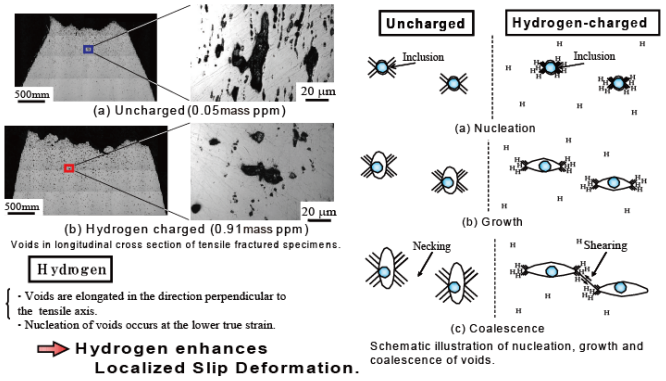

Fig.2. Development of voids in tensile test of the H-charged specimen of a pipeline steel, JIS-SGP (0.078% C)[1]

3.2 FCG behaviour of a pipeline steel[2]

Figure 3 shows slips bands morphology at crack tip for H-charged specimens tested at different frequency. Slip bands morphology for non-charged specimens was almost the same regardless of test frequency as Fig.3(a) for H-charged specimen tested at f =10Hz. The slip bands for H-charged specimen tested at f =0.01Hz are localized only near crack tip. Nevertheless, the crack growth rate of H-charged specimen is markedly accelerated at low frequency as shown in Fig.4.

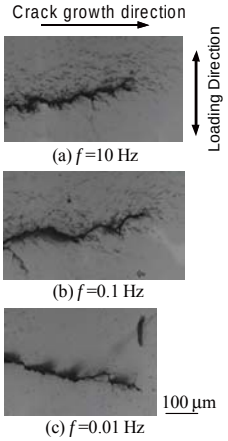

Fig.3. Crack-tip of hydrogen charged specimen.
$C_{H,R}$=1.1 ppm[2]

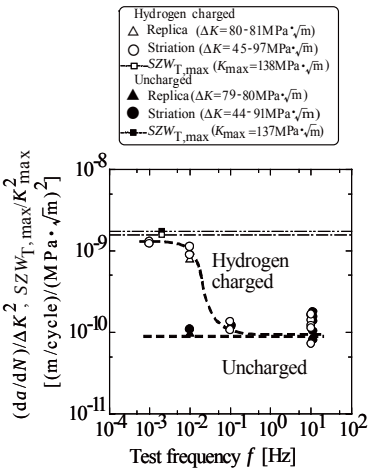

Fig.4. Relationship between crack growth rate and test frequency of 10% pre-strained specimen[2].

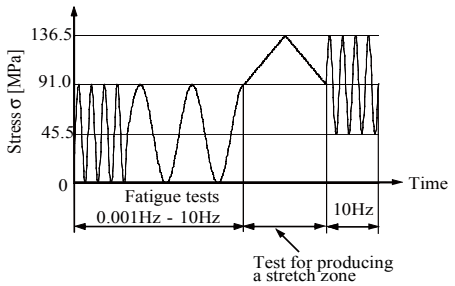

Fig.5 .Loading pattern of fatigue crack growth tests and test for producing a stretch zone[2].

In order to investigate the mechanism of crack growth acceleration mechanism, the morphology of stretch zone (Fig.6) was compared between H-charged specimen and uncharged specimen by applying the load spectrums shown in Fig.5. The maxim size of stretch zone size ($SZW_{T,max}$) was measured by tilting fracture surface. If crack tip blunting is large, large tilting angle is necessary for measurement of $SZW_{T,max.}$ The measured tilt angles in uncharged and H-charged specimen revealed the peculiar crack grow mechanism in presence of hydrogen as illustrated in Fig.6(b).

3.3 Effect of hydrogen on fatigue behaviour of a Cr–Mo steel SCM435[3]

As shown in Fig.7, the crack growth rates under hydrogen effect are 30 times higher than those for uncharged specimens.

The slip bands of the H-charged specimens were localized only at very narrow area beside the crack line. These characteristics are commonly observed in H-charged specimens of other materials[4].

3.4 Effect of hydrogen on fatigue behaviour of austenitic stainless steels

3.4.1 Effect of hydrogen on fatigue crack growth in solution treated austenitic stainless steels.

Figure 8[4] shows FCG curves starting from a hole in the uncharged and H-charged specimens of Type 304, Type 316 and Type 316L. For both Type 304 and Type 316, the increased FCG rate due to increased H-content is clear. The crack growth rate in the H-charged Type 316L was only slightly higher than the uncharged Type 316L. It must be noted that the fatigue tests of Fig.8 were performed at frequencies f of 1.2-5 Hz.

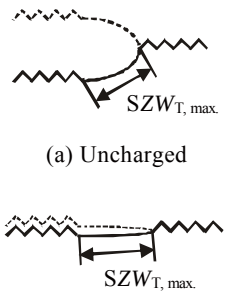

Fig.6. Difference in morphology of stretch zone for uncharged and H-charged specimen[2].

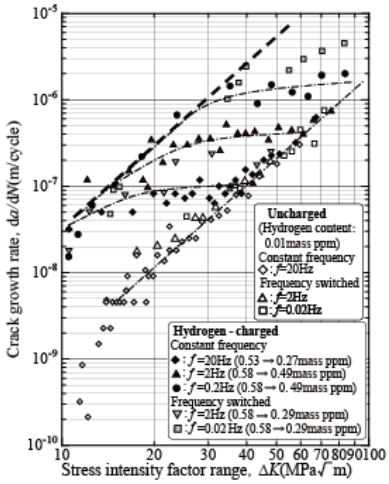

Fig.7. Relationship between da/dN and ΔK. Material: SCM435[3]. Hydrogen content indicated by ∗∗→∗∗∗ means that hydrogen content decreased from∗∗∗ to ∗∗ during fatigue test. ‘‘Frequency switched” means that the test frequency was switched between f = 2 Hz and f = 0.02 Hz.

3.4.2 Effects of hydrogen and test frequency on fatigue crack growth

Figure 9(a) and (b) [5]shows the crack growth curves for Type 304 and Type 316L specimens. Fig. 9(c)[5] shows the da/dN, and ΔK, for Type 316L. In Type 316L tested at a frequency of 1.5 Hz, there was no pronounced difference between the H-charged specimen and the uncharged specimen. The FCG rates of the H-charged Type 316L, tested at f = 0.0015 Hz, were 2–3 times higher than those of Type 316L tested at f = 1.5 Hz. Surprisingly, the uncharged specimen also exhibited an obviously definite crack growth rate increase as f decreased from 1.5 Hz to 0.0015 Hz.
In Type 304 as well as in Type 316L, the uncharged specimen exhibited a definite frequency effect. As the f decreased from 1.2 Hz to 0.0015 Hz, FCG rates increased (Fig.9 (a)).

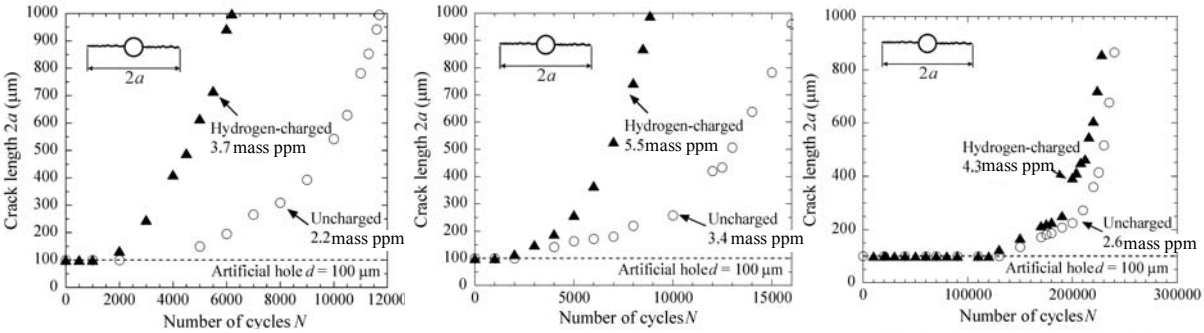

(a) Type 304 (σ = 280MPa, f = 1.2 Hz) (b) Type 316 (σ = 260MPa, f = 1.2 Hz) (c) Type 316L (σ = 260MPa, f = 5 Hz)

Fig.8. Influence of H-charging on crack growth from 100 μm hole for austenitic stainless steels Type 304, Type 316 and Type 316L. H-charging was carried out by cathodic charging at 50 ^{o}C for 672 h[4].

.

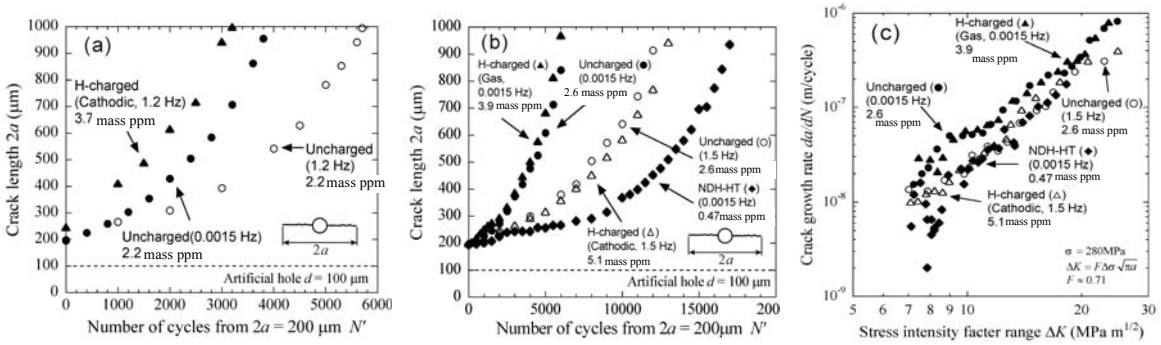

(a) Type 304 (σ = 280MPa) (b) Type 316 (σ = 280MPa) (c) Type 316L

Fig.9. Influence of hydrogen and test frequency on crack growth from $2a$ = 200μm [5] .

3.4.3 What happens if non-diffusible hydrogen is removed by the special heat treatment?

In order to investigate the influence of so-called non-diffusible hydrogen which is unavoidably trapped in the material steel process on FCG, a special heat treatment named NDH-HT was applied[5]. The effect of NDH-HT is clearly shown in Fig.10, in which the hydrogen content in an ordinarily heat treated Type 316L is 2.6 mass ppm, and on the other hand in the sample subjected to NDH-HT the content is 0.4 mass ppm.

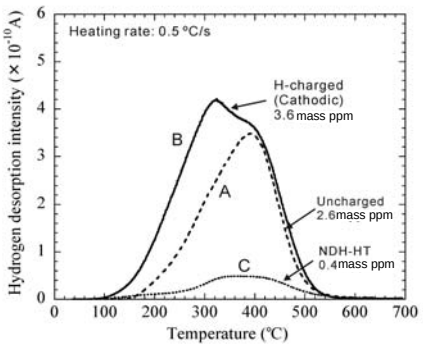

Fig.10. Hydrogen thermal desorption spectrum of Type 316L[5].

Fig.9 (b) shows the FCG behaviour of NDH-HT specimens. Surprisingly, the FCG rate of an NDH-HT specimen was substantially decreased in comparison with a H-charged specimen, and even in comparison with an uncharged specimen. Further evidence of the effect of NDH-HT was seen in the striation height-spacing ratios (*H/s*) which are shifted to higher values. The above facts are the definite proof that even the non-diffusible hydrogen contained in ordinary solution treated austenitic stainless steels influences FCG rates.

3.4.4 Hydrogen-induced striation formation mechanism and FCG mechanism

Figure11 (a) and (b) illustrate the effect of hydrogen on the crack closure mechanism during one load cycle. Figure 11 ((a-1) → (a-4)) shows the crack opening behaviour on the way to the maximum load in the absence of hydrogen. The crack tip opening displacement reaches its saturated value at a given load level and crack growth ceases. As shown in Fig.11 ((b-1) → (b-2)), however, hydrogen concentrates near the crack tip in the presence of hydrogen. Hydrogen concentration enhances further crack opening by slip, and crack growth continues. Since the corresponding plastic zone at the crack tip does not become large, the plastic zone wake which remains on the fracture surface is shallow. The difference in crack tip blunting mechanism between no H-effect and H-effect is essentially the same as Fig.2. Figure 11 (c) and (d) are schematic illustrations of plastic zone wakes with and without hydrogen. This phenomenon results both in decrease in the height of striation and in decrease in the crack opening load (decrease in ΔK_{op} and increase in ΔK_{eff}).

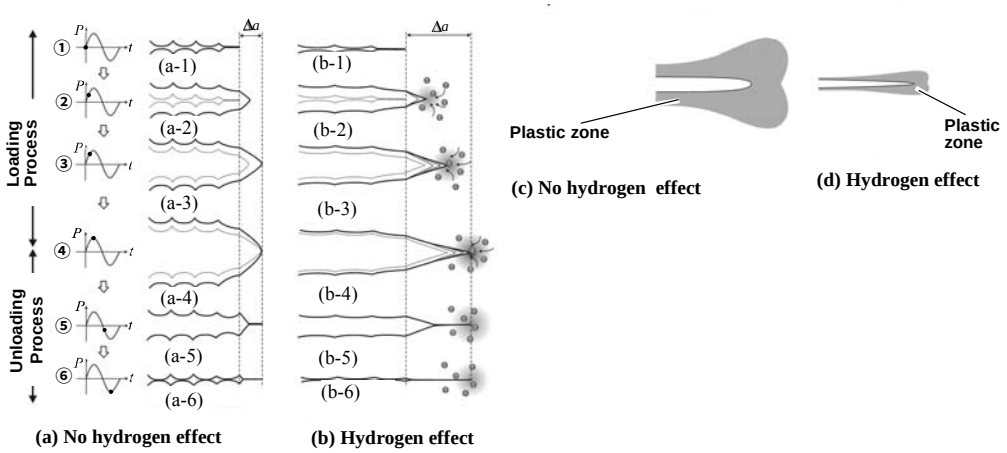

Fig.11 .Crack tip opening and striation formation mechanism in fatigue[5]

3.4.5 Hydrogen Effect against Hydrogen Embrittlement

As described in the previous section, in the uncharged specimens, many grains were covered with slip bands around a fatigue crack, while in the H-charged specimens, slip bands appeared only in the vicinity of a crack, but under the same stress, fewer slip bands were observed in grains away from the crack (see Fig.12). This phenomenon shows that hydrogen increased the resistance against crystallographic glide, i.e., hydrogen hindered dislocation motion, eventually leading to hardening. Nevertheless, FCG rates for the H-charged specimens were significantly increased compared with those for uncharged specimens.

What does this contradiction in the results of optical microscopic observations mean? Hydrogen increases macroscopic strength by slip localization, resulting in a discrete slip band arrangement, so why are FCG rates accelerated in the presence of hydrogen? One possible interpretation is that the phenomenon that occurs at the fatigue crack tip differs from slip behavior in grains away from the crack (see Fig.12). However, as shown in the detailed observations by Murakami et al.[5] and Kanezaki et al.[4], it is evident that the deformation process at a fatigue crack tip in austenitic stainless steels is based on crystallographic slip, and the fatigue crack growth is not based on a decohesion mechanism. It was shown[4] ,[5] that the fracture mechanism at a fatigue crack tip is essentially a ductile microfracture, since clear striations were observed on the fracture surfaces of H-charged specimens. The basic mechanism of the fracture process at a fatigue crack tip is slip originated by dislocation motion in crystals. Therefore, we need to recognize that the source of the mystery exists in the interaction between hydrogen and dislocations.

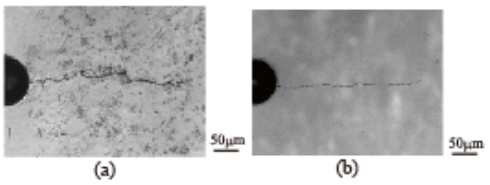

Fig.12. Macroscopic observation of slip deformation behavior around fatigue crack. (a) Uncharged type 304 at 1.0 Hz (C_H = 2.2 mass ppm, σ = 280 MPa, N = 11,000, and 2a = 0.782 mm), and (b) H-charged type 304 at 1.0 Hz (C_H = 89.2 mass ppm, σ = 280 MPa, N = 92,000, and 2a = 1.028 mm) [6]

In order to resolve the mystery of HE, we paid particular attention to the quantitative effects of H-content, ranging from an uncharged level to supersaturated levels in the material. From the term ‘‘HE’’, we presume that the higher the H-content in a material, the lower the strength properties of the material as shown in the previous section[5].

Murakami et al.[6] obtained a uniform supersaturated high H-content distribution throughout fatigue specimens by exposing types 304 and 316L specimens to gaseous hydrogen at a pressure up to approximately 100 MPa and at a temperature of 553 K (280 ^{o}C).

In tests on specimens containing supersaturated H, the authors anticipated the appearance of strong HE, but what actually happened was surprising and dramatic. It is expressed as “Hydrogen effect against HE”. The unprecedented experimental results are presented in Fig.13.

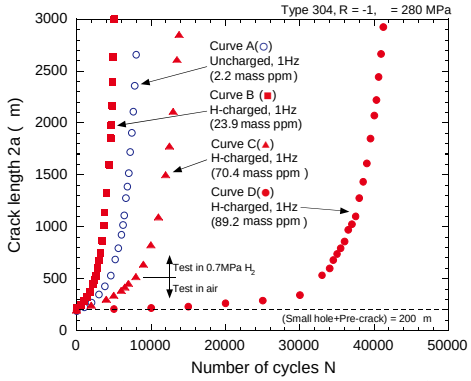

Fig.13. Effect of H-content on fatigue crack growth. Hydrogen effect against HE[6].

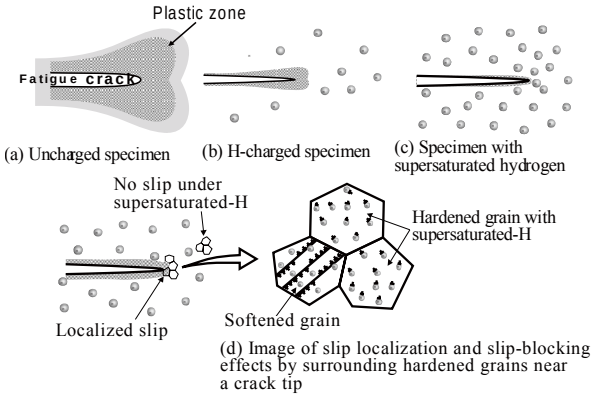

Fig.14 Schematic illustration of plastic deformation in the vicinity of fatigue crack tip. Mechanism of hydrogen effect against HE[6].

4. Positive use of HE phenomenon for inclusion rating of high strength steels[7]

4.1 Materials and specimens

The SAE52100 specimens were used for tensile testing and tension-compression fatigue testing. Figure 15 shows the dimensions and shapes of the tensile test specimen and tension-compression fatigue test specimen.

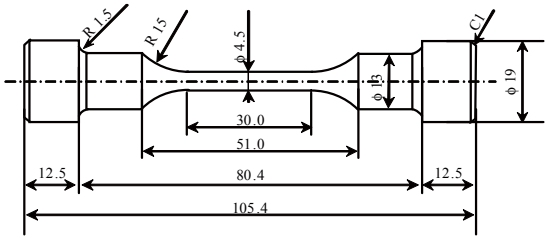

(a) Tensile test specimen, control volume: V_S = 477 mm^3
Specimen for SAE52100

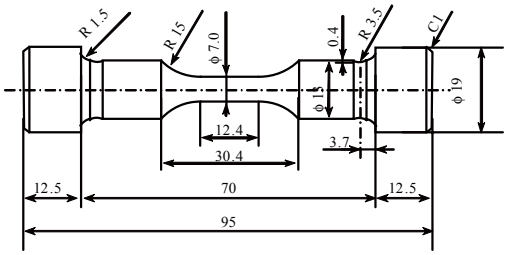

(b) Fatigue test specimen, control volume: V_S = 477 mm^3.
Specimen for SAE52100

Fig.15. Shapes of test specimens (Dimension in mm).

4.2 Hydrogen-precharge method (H-precharge method)

Specimens were H-charged by immersion in an aqueous solution of 20 mass % NH_4SCN at 313 K for 48 hours.

4.3 Tensile testing of H-precharged specimens

Tensile tests were conducted using uncharged specimens and H-precharged specimens. All tensile testings were performed in laboratory air at room temperature. Tensile test of each SAE52100 specimen was started about two hours after hydrogen charging. The control volume of the tensile test specimen (Fig.15(a)) was $V_s = (\frac{\pi}{4}) \times 4.5^2 \times 30 = 477 \text{mm}^3$. The residual hydrogen contents ($C_{H,R}$) were measured at the end of the tests.

4.4 Nonmetallic inclusion rating by the fatigue testing

Vickers hardness of the fatigue test specimen was *HV* 682. The control volume of one fatigue test specimen was $V_s = (\pi/4) \times 7.0^2 \times 12.4 = 477$ mm^3.

4.5 Inclusion rating by the HE method

Figure 16 shows an example of σ-ε curves of uncharged specimens and H-precharged specimens of SAE52100 steel.

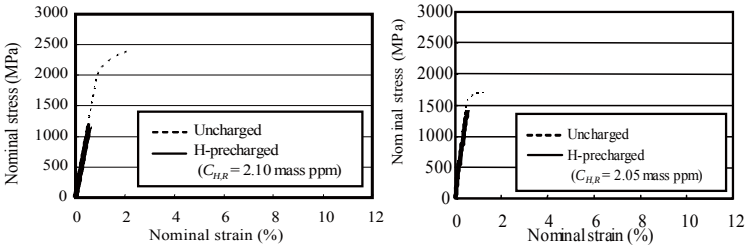

(a) Tempering temperature:513K, *HV*=678 (b) Tempering temperature:743K, *HV*=447

Fig. 16 Nominal stress-strain curves of uncharged and H-recharged specimens. Material: SAE52100, Cross head speed: 1mm/min, Time from the end of H-precharge to the start of tensile test: 2 h, $C_{H,R}$: Residual hydrogen content.

Figure 17 compares the fracture surfaces for uncharged specimens and H-precharged specimens. The mating surfaces at the fracture origin are also shown in Fig17.

Figures 17 (a) shows that the uncharged specimens also fractured from nonmetallic inclusions, TiN. In case of uncharged specimens, Fig. 17 (a-2) and 17 (a-3), fracture origins are TiN inclusion. This fact implies that TiN inclusions in the uncharged specimens were cracked under plastic deformation in tensile test because TiN inclusions cannot adapt to large plastic deformation of the matrix. As shown in Fig.16, uncharged specimens with a hardness even higher than *HV* 447 were fractured with plastic deformation after yielding. It should be noted that uncharged specimens fractured from TiN inclusions which are smaller in size than Al_2O_3•$(CaO)_X$ inclusions.

On the other hand, figure 17 (b) shows a typical nonmetallic inclusion at the fracture origin of the H-precharged specimen. The nonmetallic inclusion was identified to be Al_2O_3•$(CaO)_X$ inclusion. These inclusions are typical ones contained in ordinary commercial bearing steels such as SAE52100. As shown in Fig. 17 (b-2) and Fig. 17 (b-3), the nonmetallic inclusion at the fracture origin for the H-precharged specimens exists only on one side of the fracture surface. This is evidence that the interfaces between Al_2O_3•$(CaO)_X$ inclusion and the matrix were debonded in the H-precharged specimens, and then the domain of the inclusion becomes mechanically equivalent to a void from which the crack initiated. As shown in Fig.16, H-precharged specimens with a *HV* of higher than *HV* 447 fractured before yielding.

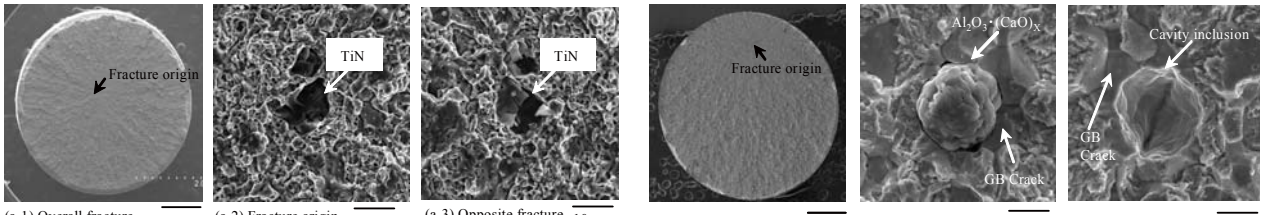

(a-1) Overall fracture surface 1 mm (a-2) Fracture origin 10 μm (a-3) Opposite fracture origin of (a-2) 10 μm

(a) Uncharged specimen, $\sqrt{area}$ = 10.9 μm (*HV* = 678, σ_f = 2523 MPa)

(b-1) Overall fracture surface 1 mm (b-2) Fracture origin 10 μm (b-3) Opposite fracture origin of (b-2) 10 μm

(b) H-precharged specimen, $\sqrt{area}$ = 18.6 μm (*HV* = 678, σ_f = 1132 MPa, $C_{H,R}$ = 2.60 mass ppm)

Fig. 17 SEM images of tensile fracture surfaces for the SAE52100 specimens. Cross head speed: 1mm/min, Time from the end of H-precharge to the start of tensile test: 2 h, $C_{H,R}$: Residual hydrogen content.

The H-precharged specimens with $HV \geq 447$ fractured from Al_2O_3•$(CaO)_X$ inclusions. The H-precharged specimen with HV=346 fractured by cup-cone type. Therefore, it is presumed that the lower limit of HV for fracture from Al_2O_3•$(CaO)_X$ inclusion in H-precharged specimens exists between HV 346 and HV 447. The value of Vickers hardness between HV=346 and HV=447 coincide with the critical hardness above which the material is very sensitive to HE[8,9] The sizes of inclusion at the tensile fracture origin for the H-precharged specimens (Al_2O_3•$(CaO)_X$ inclusion, the average $\sqrt{area}$ = 17.4 μm) are larger than that for the uncharged specimens (TiN inclusion, average $\sqrt{area}$ = 10.2 μm).

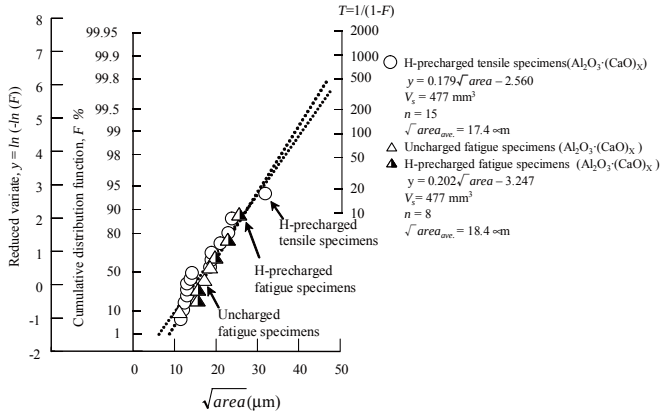

Fig. 18 Statistics of extremes distribution of Al_2O_3·$(CaO)_X$ inclusions contained in the SAE52100 H-precharged tensile specimens and fatigue testing with uncharged and H-charged specimens.

Figure 18 shows the statistics of extremes distribution of Al_2O_3•$(CaO)_X$ inclusions at the fracture origin of the H-precharged tensile specimens. Figure 18 also includes the data obtained by fatigue testing with uncharged and H-charged specimens. Here y is reduced variate, F is cumulative distribution fraction and T is return period. The graph of extreme value of $\sqrt{area}_{\max}$, of inclusions in Fig. 18 for the H-precharged specimens shows a good linearity in complete agreement with fatigue data and provides justification for the use of the distribution of extremes. This demonstrates that the maximum inclusion contained in a tensile specimen of SAE52100 can be detected by the HE method with $HV \geq 447$.

5. Conclusions

***Conclusions for a pipeline steel*:**
The difference in the morphology of stretch zone at fatigue crack tip in uncharged specimens and H-charged specimen quantified the unique crack process in H-charged specimen which is the basic mechanism of HE in low strength steels.

***Conclusions for a Cr–Mo steel*:**
With decreasing load frequency, the fatigue crack growth rate for the H-charged specimens increased significantly. However, there is the upper bound of the acceleration of da/dN and it is about 30 times of da/dN for uncharged specimens.

***Conclusions for austenitic stainless steels*:**
1. Although one of the major models assumed to explain HE has been the hydrogen decohesion hypothesis, the basic phenomenon of HE during fatigue loading is not caused by lattice decohesion. The basic mechanism is hydrogen diffusion to, and concentration at, crack tips. This leads to the activation of hydrogen induced slip deformation.
2. Fatigue crack growth rates are increased in the presence of hydrogen, and are strongly dependent on cyclic load frequency. The dependency on load frequency is a consequence of the very low hydrogen diffusion rate in austenitic stainless steels, which have the FCC structure.

3. The so-called non-diffusible (irreversible) hydrogen at a level of 2–3 mass ppm, which is trapped in the lattice of ordinarily heat-treated austenitic stainless steels, definitely increases fatigue crack growth rates when the loading frequency is reduced to 0.0015 Hz.
4. If the non-diffusible hydrogen is removed, down to the level of 0.4 mass ppm, by a special heat treatment (NDH-HT), then the damaging influence of the loading frequency disappears, and fatigue crack growth rates are significantly decreased.
5. The H-enhanced localized and discrete slip at fatigue crack tips changes the mechanism of crack opening and closing behaviour, and also produces a unique striation morphology in the presence of hydrogen.
6. Charging a supersaturated level of hydrogen drastically improves the fatigue crack growth resistance. This mysterious phenomenon has not previously been observed in the history of HE research. This finding will, not only be the crucial key factor to elucidate the mechanism of HE, but also be a trigger to review all existing theories on HE in which hydrogen is regarded as a dangerous culprit.

***Conclusions for the HE nonmetallic inclusion rating*:**

The HE-method is more convenient and reliable than other inclusion rating methods such as fatigue and optical microscopy methods. The extreme value distributions of $Al_2O_3 \bullet (CaO)_X$ inclusions obtained by HE-method on SAE 52100 coincided with those obtained with the fatigue test. The proposed method can be applied to specimens with $HV \geq 447$.

Acknowledgement

This research has been supported by the NEDO project ‘‘Fundamental Research Project on Advanced Hydrogen Science (2006–2012)”. The author gratefully acknowledges the support of the International Institute for Carbon-Neutral Energy Research (WPI-I^2CNER) supported by the Japanese Ministry of Education, Culture, Sport, Science and Technology.

References

[1] Matsuo T, Homma N, Matsuoka S, Murakami Y, Effect of hydrogen and prestrain on tensile properties of carbon steel SGP (0.078 C-0.012 Si-0.35 Mn, mass%) for 0.1 MPa hydrogen pipelines. Trans JSME A 2008;74(744):1164–73.
[2] Matsuoka S, Tsutsumi N, Murakami Y, Effects of Hydrogen on Fatigue Crack Growth and Stretch Zone of 0.08% C low Carbone Steel Pipe, Trans.JSME ser.A, 2008, 74-748, 1528-1537.
[3] Tanaka H, Honma N, Matsuoka S, Murakami Y. Effect of hydrogen and frequency on fatigue behavior of SCM435 Steel for storage cylinder of hydrogen station. Trans JSME A 2007;73(736):1358–65.
[4] Kanezaki T, Narazaki C, Mine Y, Matsuoka S, Murakami Y. Effects of hydrogen on fatigue crack growth behavior of austenitic stainless steels. Int J Hydrogen Energy 2008;33:2604–19.
[5] Murakami Y, Kanezaki T, Mine Y, Matsuoka S. Hydrogen embrittlement mechanism in fatigue of austenitic stainless steels. Metall Mater Trans A 2008;39:1327–39.
[6] Murakami Y, Kanezaki T, and Mine Y, Hydrogen Effect against Hydrogen Embrittlement, Metallurgical and Materrials Trans. A 2010;14, 2548-2562.
[7] Fujita S and Murakami Y, A New Nonmetallic Inclusion Rating Method by Positive Use of Hydrogen Embrittlement Phenomenon, submitted in 2012.
[8] S.Fukui; Tetsu-to-Hagane, 1969, vol. 55, pp. 151-61.
[9] W.M. Garrison Jr., N.R. Moody, Hydrogen embrittlement of high strength steels, pp. 421-492 in ‘Gaseous hydrogen embrittlement of materials in energy technologies’ Vol.1, Eds. R.P. Gangloff and B. Somerday, Woodhead Publishing, 2012.